Proc. Natl. Acad. Sci. USA
Vol. 92, pp. 5530–5534, June 1995
Medical Sciences

Neural-network-based classification of cognitively normal, demented, Alzheimer disease and vascular dementia from single photon emission with computed tomography image data from brain

RUI J. P. DEFIGUEIREDO*, W. RODMAN SHANKLE†, ANDREA MACCATO*, MALCOLM B. DICK†, PRASHANTH MUNDKUR*, ISMAEL MENA‡, AND CARL W. COTMAN†

*Laboratory for Machine Intelligence and Neural Computing, Department of Electrical and Computer Engineering and †Irvine Research Unit on Brain Aging, Department of Neurology, University of California, Irvine, CA 92717; and ‡Department of Radiology and Nuclear Medicine, University of California, Los Angeles, CA 90024

Communicated by James L. McGaugh, University of California, Irvine, CA, December 27, 1994 (received for review July 15, 1994)

ABSTRACT **Single photon emission with computed tomography (SPECT) hexamethylphenylethyleneamineoxime technetium-99 images were analyzed by an optimal interpolative neural network (OINN) algorithm to determine whether the network could discriminate among clinically diagnosed groups of elderly normal, Alzheimer disease (AD), and vascular dementia (VD) subjects. After initial image preprocessing and registration, image features were obtained that were representative of the mean regional tissue uptake. These features were extracted from a given image by averaging the intensities over various regions defined by suitable masks. After training, the network classified independent trials of patients whose clinical diagnoses conformed to published criteria for probable AD or probable/possible VD. For the SPECT data used in the current tests, the OINN agreement was 80 and 86% for probable AD and probable/possible VD, respectively. These results suggest that artificial neural network methods offer potential in diagnoses from brain images and possibly in other areas of scientific research where complex patterns of data may have scientifically meaningful groupings that are not easily identifiable by the researcher.**

Alzheimer disease (AD), vascular dementia (VD), or both occur in 70–90% of all dementias and are often clinically difficult to distinguish. Brain imaging is an important part of the diagnostic evaluation (1–4). However, the brain image may be qualitatively difficult to distinguish between normal and demented persons, and more so between different dementia types such as AD and VD. Since disturbances of brain metabolism may precede structural changes, metabolic images can detect more subtle patterns of change earlier than anatomical ones. We chose single photon emission with computed tomography (SPECT) because (*i*) it provides measures of regional tissue uptake (hexamethylphenylethyleneamineoxime technetium-99 or HMPAO-^{99}Tc) that show complex patterns of brain activity and because (*ii*) it is widely available. Improvements in the recognition, quantification, and classification of these image patterns could increase diagnostic sensitivity between normal and abnormal as well as between different subtypes of dementia.

The need for better methods of diagnostic interpretation of brain images is illustrated by the large variability in their diagnostic interpretation by even well-trained neuroradiologists using standardized criteria. For example, the Consortium to Establish a Registry for Alzheimer's Disease (CERAD) conducted an interrater reliability study among 14 participating CERAD neuroradiologists for interpreting specific magnetic resonance imaging features and found within-feature correlations ranging from 0.64 (for detecting cerebral sulcal dilatation) to 0.79 (for rating the size of the lateral and third ventricles and the temporal horn) (5). They concluded, "we did not find satisfactory inter-rater agreement for interpreting MR findings in elderly subjects. More objective and reproducible procedures are needed for interpretation of neuroimaging findings of AD in multicenter studies."

One possible solution to these problems is to use artificial neural networks capable of recognizing subtle, complex, and diagnostically informative patterns of brain images. Artificial neural networks are computational models (6, 7) originally inspired by the physiological structure of the human brain. In the present investigation, we employed an optimal interpolative neural network (OINN) algorithm, described in ref. 8 and fully investigated in refs. 9 and 10, to classify such patterns of change in brain SPECT data of elderly patients. We chose an OINN because it minimizes the use of redundant information in the image data, improves with training (evolutionary), and can generate highly nonlinear decision boundaries, allowing it to maximize the use of small training samples.

In this application, the SPECT image data of carefully diagnosed and well-characterized patients were divided into training and testing samples. After aligning, normalizing, and partitioning these images into regions of interest (ROIs), vectors composed of a patient's ROIs (feature vectors) were created to train and test the OINN. Given the diagnosis of each patient in the training sample, the OINN processed their feature vectors, stored in the first layer of the network, to create a second layer of nodes possessing weighted coefficients that help discriminate the different diagnoses for which the network is being trained. After the OINN has been trained, each patient's feature vector in the testing sample enters the network and is "diagnosed" by the third layer of the network, the output layer, by using the information from the second layer. The correct classification percentage is then computed for each diagnosis as a means of evaluating the algorithm's performance.

METHODS

Patient Selection. In the present study, the clinical criteria employed for the diagnosis of probable AD and VD are much

The publication costs of this article were defrayed in part by page charge payment. This article must therefore be hereby marked "*advertisement*" in accordance with 18 U.S.C. §1734 solely to indicate this fact.

Abbreviations: AD, Alzheimer disease; VD, vascular dementia; OINN, optimal interpolative neural network; SPECT, single photon emission with computed tomography; HMPAO-^{99}Tc, hexamethylphenylethyleneamineoxime technetium-99; ROI, region of interest; NINDS-ADRDA, National Institute for Neurological Disorders and Stroke/Alzheimer's Disease and Related Disorders in Aging; MMSE, mini-mental state exam; CERAD, Consortium to Establish a Registry for Alzheimer's Disease.

improved over previous methods. The criteria for VD were modeled after the Alzheimer's Disease Diagnosis and Treatment Centers (ADDTC) criteria (11) to specifically distinguish patients with probable or possible VD from those diagnosed as probable AD patients based on National Institute for Neurological Disorders and Stroke/Alzheimer's Disease and Related Disorders in Aging [NINDS-ADRDA] criteria. Part of this distinction is based on magnetic resonance imaging findings. By using these criteria for the clinical diagnosis of probable AD [NINDS-ADRDA (12)] and probable/possible VD [Alzheimer's Disease Diagnostic and Treatment Centers (11)], we selected samples of 20 probable AD patients, 22 probable and possible VD patients, and 25 elderly control patients who had SPECT scans at the same center and were interpreted by the same SPECT diagnostician. Each demented patient was evaluated at the UC Irvine Alzheimer's Disease Research Center with a standardized diagnostic protocol, consisting of routine laboratory screens for causes of dementia, chest x-ray, electrocardiogram, magnetic resonance imaging, history, caregiver interview, physical and neurological examinations, and 2 h of cognitive testing using the CERAD battery (13) and other selected neuropsychometrics. To provide the OINN with the clearest examples having the highest probability that the clinical diagnosis was correct, we only selected patients who had a clearcut clinical diagnosis of probable AD and probable or possible VD and excluded patients who met criteria for both AD and VD. Diagnosis was made by consensus among the clinical team who evaluated the patient. Controls were selected who had no history of cognitive or functional impairment and who had a Folstein mini-mental status examination (MMSE) score >29 out of 30. The demographics (age at onset, symptom duration at time of SPECT study, sex, years of education, and MMSE score) of the AD and VD groups appear in Tables 1 and 2.

To select a patient sample for our analysis, we examined for differences in descriptive characteristics (age at onset, symptom duration, sex, years of education, and MMSE) among the AD, VD, and control groups by using the exact Bonferroni test. This test adjusts the type I error (α) to a specified probability

Table 1. Characteristics of the AD samples

Diagnosis	Age at onset, yr	Symptom duration, yr	Sex	Education, yr	MMSE score, no./30
Prob AD	61	0.72	M	11	19
Prob AD	77	1.10	M	16	21
Prob AD	73	2.39	F	14	19
Prob AD	63	2.49	M	12	10
Prob AD	63	2.52	M	12	14
Prob AD	73	2.89	F	9	22
Prob AD	70	3.04	F	14	0
Prob AD	86	3.11	F	10	17
Prob AD	72	3.47	F	13	17
Prob AD	60	3.67	F	12	5
Prob AD	54	3.82	M	14	16
Prob AD	64	4.97	M	16	6
Prob AD	71	5.24	F	12	18
Prob AD	54	5.89	M	12	16
Prob AD	72	6.34	F	13	20
Prob AD	70	6.37	F	14	15
Prob AD	66	6.77	M	16	6
Prob AD	61	7.96	M	13	12
Prob AD	67	8.82	F	19	23
Prob AD	78	8.88	M	12	14
Statistics of AD group (n = 20)					
Mean	67.80	4.523	50% M	13.20	14.50
SD	8.04	8.296		2.31	6.25

Prob, probable; M, male; F, female.

Table 2. Characteristics of the VD samples

Diagnosis	Age at onset, yr	Symptom duration, yr	Sex	Education, yr	MMSE score, no./30
Prob VD	72	0.11	F	12	22
Prob VD	81	0.17	F	19	22
Prob VD	85	0.47	F	8	20
Prob VD	83	0.53	M	3	20
Prob VD	74	0.72	M	12	18
Poss VD	77	0.74	F	4	15
Poss VD	75	0.96	M	10	18
Prob VD	79	1.97	F	16	27
Poss VD	71	2.64	M	13	24
Poss VD	87	2.76	M	12	13
Poss VD	88	3.15	M	16	26
Poss VD	62	3.19	F	10	23
Poss VD	74	3.28	F	12	22
Poss VD	56	3.46	M	19	21
Prob VD	76	4.06	F	12	14
Prob VD	78	4.33	F	17	21
Prob VD	73	4.78	M	19	27
Poss VD	61	5.15	F	13	26
Prob VD	62	5.55	F	13	25
Prob VD	71	7.63	F	8	15
Poss VD	65	8.70	F	16	14
Prob VD	65	13.60	M	19	25
Statistics of VD group (n = 22)					
Mean	73.40	3.55	40% M	12.90	20.80
SD	8.81	7.75		4.58	4.49

Prob, probable; M, male; F, female.

(we chose 0.05) when one simultaneously tests multiple variables for significant differences between groups. There was no significant difference between the AD and VD groups for any of these descriptive variables (age at onset, $P = 0.02$; symptom duration, $P = 0.171$; sex, $P = 0.556$; education, $P = 0.758$; MMSE score, $P = 0.0004$; overall, $P = 0.0816$). For the controls, their MMSE score was by definition significantly different because they had to have a score >29 to be a control. Their age was 67.3 ± 8.22 (mean ± SD), which is not significantly different statistically from either disease group ($t = 0.062$, $P = 0.50$ for AD vs. control; $t = 0.725$, $P = 0.80$ for VD vs. control). Age at onset and symptom duration were not applicable to the controls.

SPECT Images. The SPECT scans done on each patient were an HMPAO-^{99}Tc 8-mm-resolution SPECT acquired at Harbor-UCLA Hospital by using a Shimadzu scanner. The HMPAO-^{99}Tc method yields 11 transverse slices parallel to the orbitomeatal reference plane, of which 7 slices above the orbitomeatal plane were selected for analysis. It measures relative regional tissue uptake acquired over 1 h, and the resulting scintillation counts are expressed as the percentage of the maximal counts in the brain. Typically, these are translated to a color scale for visual inspection of the distribution of HMPAO-^{99}Tc uptake. These data were subjected to tomographic reconstruction and then subjected to image registration, normalization, and feature extraction, prior to the analysis by the OINN.

SPECT Image Registration. The registration and normalization of SPECT images were accomplished by a model-based procedure driven by a correlation criterion and an iterative optimization program. The algorithm performs a six-parameter registration of the images, accounting for uniform scaling, translation, and rotation in the image plane, and for discrete translation perpendicular to the image plane. The procedure was applied to all images in the database. For the purpose of illustration, registered scans of the seventh (middle) HMPAO-^{99}Tc slice for typical control, AD, and VD subjects are shown in Fig. 1.

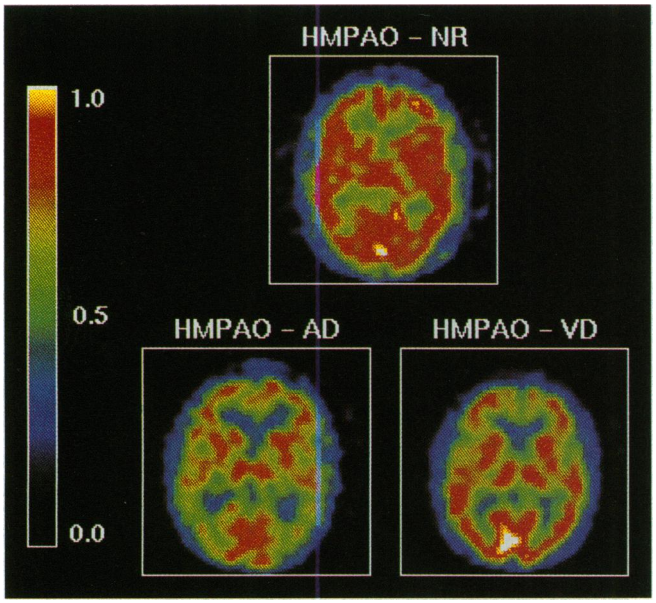

FIG. 1. HMPAO-^{99}Tc registered scans. The seventh slice is shown for typical control (NR), AD, and VD subjects.

SPECT Feature Vector Selection. After registration, each of the seven HMPAO-^{99}Tc slice images was mapped to three xenon-equivalent slice images at 2, 4, and 6 cm above and parallel to the orbitomeatal plane. These three slices of combined HMPAO-^{99}Tc slices were divided into 19 ROIs (regional masks), whose mean tissue uptake values were transformed into a feature vector, $\{x_j\}$, to be analyzed by the OINN. These 19 ROIs consist of aggregates of the ROIs previously used by ref. 14 and correspond to four frontal, two frontotemporal, four temporal, three parietal, three occipital, and three ventricular areas (Fig. 2). For the classification of demented vs. normal aging, the training and testing samples were then constructed using these 19-component feature vectors as input to the OINN. For the classification of AD vs. VD, a reduced number of component feature vectors were selected by running all possible pairs of ROI through the OINN, then selecting the four ROIs that provided the best discrimination with this paradigm. The training and testing samples were then constructed by using these four-component feature vectors as input to the OINN.

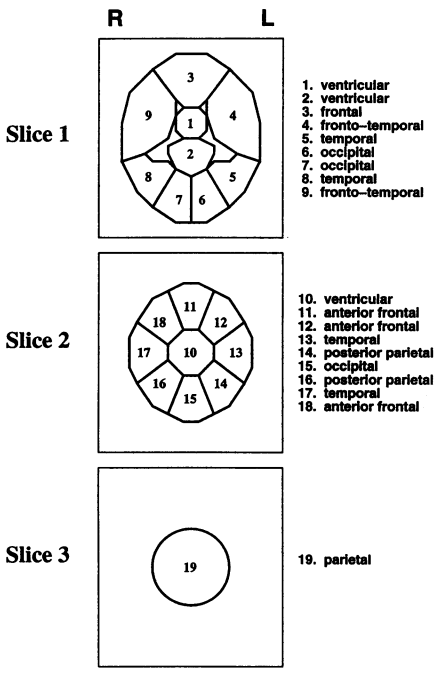

FIG. 2. ROI masks used to extract average intensity features from the SPECT scans.

OINN CLASSIFIER ALGORITHM

Training and Test Sample Selection. To classify patients based on their SPECT feature vectors, distinct samples of patients from each diagnostic category were selected to train and test the net. A jackknifing method (15) was used to create a series of training and testing samples. For each training and testing sample created, one patient was selected to test the net, while the rest of the sample trained the net. To allow comparability with linear discriminant functions, we decided to create two OINNs, one to diagnose demented vs. cognitively normal elderly persons and the other to diagnose AD vs. VD patients. For the first net, all 67 patients could be used to create 67 sets of training and testing patient samples. For each of the 67 sets, 66 patients' SPECT feature vectors trained the net and one patient's feature vector tested this trained net. Then, each test patient's OINN classification was compared to the clinical diagnosis (demented vs. nondemented) and the correct classification percentage was computed. For the second net, the 42 patients clinically diagnosed as AD or VD were used to create 42 sets of training and testing patient samples. For each of the 42 sets, the test patient's OINN classification was compared to the clinical diagnosis (AD vs. VD) and the correct classification percentage was computed.

Layers of the OINN. As depicted in Fig. 3, the OINN has an input layer (layer 1) that receives the feature vector $\{x_j\}$. A set of transformation coefficients maps layer 1 into the second layer (layer 2), which encodes the similarity measure of each patient's input feature vector to a set of predetermined prototype feature vectors. The second set of transformation coefficients maps the similarity measures of layer 2 into an output layer of values that encode the classification of the input feature vector. By using a k-means clustering algorithm with all patients in the training sample of each diagnostic category, the first set of transformation coefficients $\{v_{ij}\}$ are independently computed for each diagnosis being classified by that net. The second set of transformation coefficients $\{w_j\}$ is obtained by minimizing the squared error over the training sample. During training, the network coefficients are calculated in closed form by an optimal interpolating algorithm that minimizes a generalized fock space norm of the input–output map of the net.

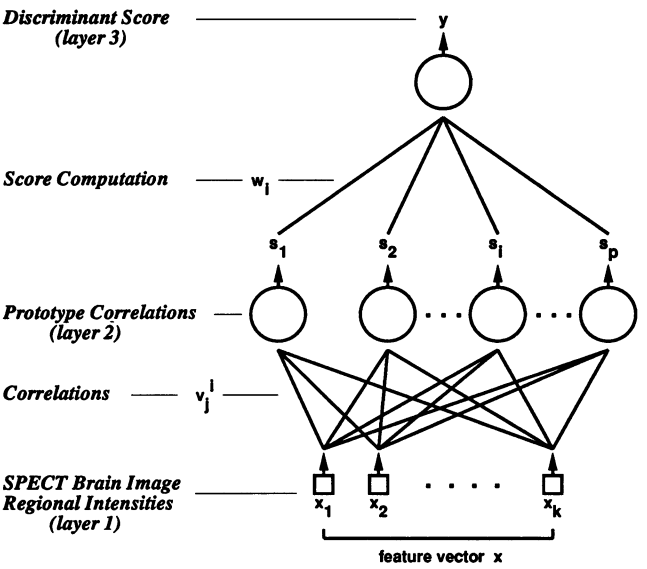

FIG. 3. OINN structure diagram.

In the context of fuzzy logic formalism, the gain parameter γ helps control the crispness of the classification boundary surface. The sampling method of jackknifing (discussed later) helps determine the range of γ and other modifiable network parameters that will provide robust classifications. In summary, the classification output y is computed from each test sample feature vector $\{x_j\}$ as follows:

$$y = \sum_i w_i exp(\gamma \sum_j v_{ij} x_j). \quad [1]$$

RESULTS

SPECT Image Registration for the OINN. As a means to evaluate the accuracy of registration, the distances between specific internal landmarks (the anterior-most and posterior-most points of the interhemispheric fissure, and the anterior points of the Sylvian fissure) of the preregistered and the average prototype SPECT scan were measured. These distances were then compared to the postregistered images of the same set of patients, and a percentage reduction in distance from these internal landmarks was computed. The results show that there was an average 48% reduction in error due to alignment and positioning after image registration.

Feature Vector Selection for AD vs. VD Discrimination. By using all possible pairs of ROIs, the four areas that provided the best discrimination for AD vs. VD were the left parietal and the left and right temporal and posterior ventricular regions. These four regions were then used together to best discriminate AD vs. VD by using the OINN.

For the OINN diagnosing dementia vs. cognitively normal elderly, all 19 ROIs were used on the sample of 67 subjects (25 cognitively normal elders and 42 demented patients). The net was consistently trained with the gain parameter γ set to 1, and one cluster per class was requested of the k-means cluster algorithm. For the OINN diagnosing AD vs. VD, the number of ROIs had to be reduced because of the smaller data sample available (20 AD and 22 VD patients). We selected four ROIs that appeared to be particularly useful for this classification task. Again, the gain parameter γ was consistently set to 1, but the number of clusters per diagnostic class used with the k-means algorithm was increased to five.

Selecting the Prototype Feature Vectors. In computing the transformation coefficients between layers 1 and 2 v_{ij}, which are based on the prototype feature vectors, we found the spacing provided by a k-means clustering algorithm to give robust results. For each diagnostic group to be classified, we used a k-means clustering algorithm to compute v_{ij}. This algorithm uses a similarity measure, over the set of training sample feature vectors, to compute a set of k prototype vectors. The prototype vectors represent well-spaced feature vectors distributed throughout the input SPECT training sample, such that spatially isolated vectors are represented individually, while feature vectors clustered together are represented collectively by one or a few of the k prototype vectors in the corresponding diagnostic group. The resulting prototype vectors, representing either the centers of feature vector clusters or isolated feature vectors, give all the SPECT input data an opportunity to influence the shape of the final classifier function. The k prototype vectors from each diagnostic group are then assembled to constitute the transformation coefficients v_{ij}. In our analysis, the value of k was specified a priori as a network parameter.

We chose to minimize the total number of classification errors. To this end, the sample output values, used in calculating the solution of the second set of transformation coefficients w_i, were set equal to $+1/(N_a)^{1/2}$ and $-1/(N_b)^{1/2}$, respectively, for the patient samples belonging to classes a and b (demented vs. control and AD vs. VD, respectively). N_a and N_b are the number of patients in classes a and b, respectively, for the training sample. This weighting strategy for the samples appears to provide good results for unequal class sizes.

Creation of Training and Testing Samples. We validated the classification results obtained by the OINN by always training and testing the net on distinct data samples. Because of the limited size of the data set, we used a discrimination and validation strategy consisting of a modification of the jackknifing procedure (15). Its use helped constrain the modifiable network parameters, γ and the number of clusters per class, into a range of values that provided robust classification results for the specified task. We formed a collection of training data subsets by eliminating each patient in turn. This gave rise to 42 data subsets, each consisting of 41 training vectors and one test vector. The algorithm was trained on each training data subset independently, and the resulting discrimination was tested on the test vector.

Classification by the OINN. A parallel set of experiments using linear discriminant analysis showed it to be inadequate in classifying these groups. We then used the OINN with its nonlinear decision boundary abilities and found that two networks gave the best classification results. The first network classified whether a patient in the testing sample was demented or not, and correctly classified 63 of 67 samples correctly (correct classification is 94% for both groups, 98% for demented, and 88% for nondemented). As previously stated, by using only four ROIs per feature vector, the second network tested only patients clinically diagnosed as demented due to AD or VD. It correctly classified 35 of 42 samples (correct classification is 83% for both groups, 80% for AD, and 86% for VD). Among the regions selected, the data suggest that the AD group had less HMPAO-^{99}Tc-mediated tissue uptake in the left parietal cortex relative to other cortical areas of the same patient than did the VD group.

Effect of Data Jackknifing. In addition to the jackknifed validation experiments, an additional series of experiments was also performed. In these experiments, the patient sample was randomly divided into training and testing subsets, in three proportions: 50/50%, 75/25%, and 90/10%. In each case, 50 permutations were tried. The average performance of the OINN in learning to classify the samples was recorded in each case.

The results display a gradual deterioration in performance of the classifier as the training sample subset is reduced. For demented vs. nondemented patients, the correct classification rates corresponding to the three proportions above were 88, 92, and 94%. For AD vs. VD, the corresponding rates were 80, 82, and 84%. These results suggest that the OINN performance may increase with additional data.

DISCUSSION

Although there are a number of studies comparing SPECT HMPAO-^{99}Tc activity patterns in elderly controls and AD and VD subjects (16–19), there are few studies that independently diagnosed them with SPECT (17) and no studies using artificial neural networks to automate the SPECT diagnosis. The diagnostic accuracy of the OINN automated approach (94% correct for control vs. demented and 83% for AD vs. VD). This compares favorably to the diagnostic classification on this set of cases by the SPECT diagnostician and previous reports using SPECT (17). These results suggest that neural network algorithms have a clinical use in interpreting SPECT and presumably other modalities that can reliably reproduce the image patterns of a subject studied under the same conditions. They may also be used in research to delve further into pattern differences among specific dementias that may have pathophysiological significance.

How does the OINN work? First, the number of pertinent features of the input data must be selected in some way. Next, the net is trained to discriminate the classes of interest. The transformation coefficients between layers 1 and 2 compare

the similarity of the input data to a predetermined set of prototype vectors. In this study, the *k*-means clustering algorithm was used to select the prototypes. The result of the comparison produces a set of similarity scores that are combined in the second layer to give a number representing the most likely class to which the input data belong. The magnitude of this number is a measure of the degree of confidence of the classification by the OINN.

To achieve the high levels of correct classification in this study using the OINN, several methodological problems were addressed. Errors due to image registration were reduced by 48% to minimize artifacts at this level. To maximize the use of the available samples, the jackknifing sampling method made the most use of the available data in finding robust classification algorithms. The use of the *k*-means clustering algorithm to select prototype cases preserved the selection of less frequent patterns of brain tissue activity as prototypes that would otherwise have been averaged out by other methods. Finally, classification errors due to training the net with clinically misdiagnosed patients was minimized by only accepting patients into the sample who had a full comprehensive assessment and who clearly met the diagnostic criteria used for AD and VD by consensus among the evaluating clinical team.

It also must be recognized that the clinical diagnosis is not absolutely accurate. The probability of a clinical diagnosis of probable AD in a patient with definite AD neuropathology is >90% when NINDS-ADRDA criteria are used (20). The diagnostic agreement between VD clinically and neuropathologically cannot be easily determined since there are no well-established neuropathological criteria for VD. At present, cases available for autopsy validation are insufficient to definitively confirm the diagnosis by neuropathological measures. However, regardless of the agreement between a patient's clinical and neuropathological diagnoses, the Alzheimer's Disease Diagnostic and Treatment Centers and NINDS-ADRDA, criteria used to clinically diagnose probable/possible VD and probable AD, respectively, do separate the patients into relatively distinct clinical syndromes. In this study, patients conforming to these clinical diagnoses had patterns of HMPAO-^{99}Tc-mediated uptake into brain tissue that were indistinguishable by the OINN. Once trained, it consistently classified patients into their closely related diagnostic categories.

The data of this study suggest that, in the AD group compared to the VD group, there is poorer uptake of HMPAO-^{99}Tc into the left parietal cortex relative to the other cortical areas studied in the same patient. This finding may represent bias in a nonrandomly selected sample of either or both syndromes. Analysis of differences between disease and control groups showed no significant difference for age at onset, symptom duration, sex, years of education, and MMSE score, although there was a trend for VD patients to be less demented than AD patients.

Alternatively, the greater left parietal cortical hypoperfusion in AD vs. VD may present a piece of the neurobiological puzzle concerning differences between AD and VD. If VD is a syndrome with multiple underlying causes, and overlaps with AD (21), then the OINN may be detecting differences between one or more of these underlying VD causes and one or more of the AD causes if AD is also a syndrome.

Do cognitive studies of mild AD and mild VD support earlier involvement of functions associated with left parietal cortical dysfunction for AD patients? Mild AD patients are more impaired in verbal comprehension, delayed recall, and recognition memory (22), whereas mild VD patients are more impaired in tasks associated with frontal cortical dysfunction (23), providing some evidence supporting earlier involvement of left parietal dysfunction in AD than in VD.

In conclusion, artificial neural network algorithms offer great potential for improving the diagnostic precision of tests having complex patterns of data that are difficult for the trained human observer to discriminate. An attractive feature of this approach is that it is more quantitative, it can be updated with advancing knowledge, and it minimizes inter- and intraobserver differences in scan interpretation, allowing one to focus either on developing corrections for differences between scan protocols or on standardizing them or identifying areas of difference in interpretation. This approach offers at least a partial solution to the problem of relatively poor interobserver agreement seen even with well-standardized semiquantitative protocols. These findings, however, need to be validated with a larger and randomly selected sample and with longitudinal studies of carefully selected patients exemplary of a particular clearly definable category of interest. Given that the diagnostic groups studied represent clinical syndromes with potentially multiple etiologies, the pattern recognition accuracy for these syndromes (94% for demented vs. nondemented and 83% for AD vs. VD) makes pattern recognition methodology a powerful tool that can be used to analyze complex patterns of data and to assist researchers in discovering subtleties within them. Such methods can integrate information to provide more comprehensive chunks of data for the human gestalt to ponder and discover.

This work was supported by a National Institutes of Health/National Institute on Aging Grant AG05142 and grants from the Newcomb Family Foundation and the Oxnard Foundation.

1. Riege, W. H. & Metter, E. J. (1988) *Neurobiol. Aging* **9,** 69–86.
2. Ettlin, T. M., Staehelin, H. B., Kischka, U., Ulrich, J., Scollo-Lavizzari, G., Wiggli, U. & Seiler, W. O. (1989) *Arch. Neurol.* **46,** 1217–1220.
3. Pardo, J. V., Fox, P. T. & Raichle, M. E. (1991) *Nature (London)* **349,** 61–64.
4. Shedlack, K. J., Hunter, R., Wyper, D., McLuskie, R., Fink, G. & Goodwin, G. M. (1991) *Psychol. Med.* **21,** 687–696.
5. Davis, P. C., Gray, L., Albert, M., Wilkinson, W., Hughes, J., Heyman, A., Gado, M., Kumar, A. J., Destian, S., Lee, C., *et al.* CERAD, Part III (1992) *Neurology* **42,** 1676–1680.
6. Hopfield, J. J. (1982) *Proc. Natl. Acad. Sci. USA,* **79,** 2554–2558.
7. Shriver, B. D. (1988) *IEEE Comp.* **21,** 8–9.
8. deFigueiredo, R. J. P. (1990) *Proc. Intl. Joint Conf. Neur. Net.* **3,** 909–916.
9. Sin, S. K., deFigueiredo, R. J. P. (1992) *IEEE Trans. Neur. Net.* **3,** 315–323.
10. deFigueiredo, R. J. P. (1992) in *Artificial Intelligence, Expert Systems, and Symbolic Computing,* eds. Houstis, E. & Rice, J. R. (Elsevier, Amsterdam), pp. 303–319.
11. Chui, H. C., Victoroff, J. I., Margolin, D., Jagust, W., Shankle, R. & Katzman, R. (1992) *Neurology* **42,** 473–480.
12. McKhann, G., Drachman, D., Folstein, M., Katzman, R., Price, D. & Stadlan, E. M. (1984) *Neurology* **34,** 939–944.
13. Heyman, A., Fillenbaum, G. G. & Mirra, S. S. (1990) *Aging* **2,** 415–424.
14. Goldenberg, G., Podreka, I., Suess, E. & Deecke, L. (1989) *J. Neurol.* **236,** 131–138.
15. Efron, B. & Gong, G. (1983) *Am. Stat.* **37,** 36–48.
16. Kawabata, K., Tachibana, H., Sugita, M. & Fukuchi, M. (1993) *Clin. Nucl. Med.* **18,** 329–336.
17. Launes, J., Sulkava, R., Erkinjuntti, T., Nikkinen, P., Lindroth, L., Liewendahl, K. & Iivanainen, M. (1991) *Nucl. Med. Commun.* **12,** 757–765.
18. Gemmell, H. G., Sharp, P. F., Besson, J. A., Crawford, J. R., Ebmeier, K. P., Davidson, J. & Smith, F. W. (1987) *Comput. Assist. Tomogr.* **11,** 398–402.
19. Smith, F. W., Besson, J. A., Gemmell, H. G. & Sharp, P. F. (1988) *J. Cereb. Blood Flow Metab.* **8,** S116–S122.
20. Kazee, A. M., Eskin, T. A., Lapham, L. W., Gabriel, K. R., McDaniel, K. D. & Hamill, R. W. (1993) *Alzheimer Dis. Assoc. Disord.* **7,** 152–164.
21. Hachinski, V. & Norris, J. W. (1994) *Curr. Opin. Neurol.* **7,** in press.
22. Doody, R. S., Massman, P. & Nance, M. (1994) *Neurology* **44,** Suppl. 2, A196 (abstr. 274P).
23. Iacoboni, M., Padovani, A., Di Piero, V., Bragoni, M., Altieri, M., Rombola, G., Giannini, M. & Lenzi, G. L. (1994) *Neurology* **44,** Suppl. 2, A196 (abstr. 275P).